Accepted Manuscript

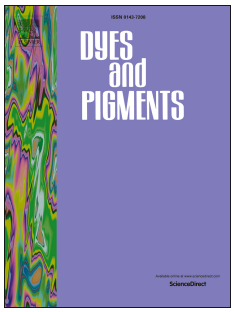

Alkoxy substituted D-π-A dimethyl-4-pyrone derivatives: Aggregation induced emission enhancement, mechanochromic and solvatochromic properties

YuQi Cao, Ye Xi, XinYu Teng, Yang Li, Xilong Yan, Ligong Chen

PII: S0143-7208(16)30864-6

DOI: 10.1016/j.dyepig.2016.09.063

Reference: DYPI 5515

To appear in: *Dyes and Pigments*

Received Date: 18 July 2016

Revised Date: 28 September 2016

Accepted Date: 29 September 2016

Please cite this article as: Cao Y, Xi Y, Teng X, Li Y, Yan X, Chen L, Alkoxy substituted D-π-A dimethyl-4-pyrone derivatives: Aggregation induced emission enhancement, mechanochromic and solvatochromic properties, *Dyes and Pigments* (2016), doi: 10.1016/j.dyepig.2016.09.063.

Alkoxy substitued D-π-A dimethyl-4-pyrone derivatives: Aggregation induced emission enhancement, Mechanochromic and Solvatochromic properties

YuQi Cao[a b], Ye Xi [a b], XinYu Teng [a b], Yang Li[a b c], Xilong Yan*[a b c], Ligong Chen*[a b c]

[a] School of Chemical Engineering and Technology, Tianjin University, Tianjin, P. R. China. E-mail: lgchen@tju.edu.cn, yan@tju.edu.cn; Fax: +86-022-27406314; Tel: +86-022-27406314

[b] Collaborative Innovation Center of Chemical Science and Engineering (Tianjin), P. R. China

[c] Tianjin Engineering Research Center of Functional Fine Chemicals, Tianjin, P. R. China

Abstract

Three series of D-π-A 2,6-dimethyl-4-pyrone-cored derivatives were designed and synthesized. Evaluation by spectroscopic methods indicated that all the compounds exhibited aggregation-induced emission enhancement (AIEE) effect and solvatochromism. The experimental results revealed that the restriction of intramolecular rotation is the key element for showcasing the AIEE phenomenon. Moreover, all of the compounds presented red-shifted mechanochromic behavior, the extent of the red-shift was mainly dependent on the position and length of alkoxyl group. The PXRD and DSC profiles demonstrated a transformation from crystalline to amorphous state upon grinding. The D-A strategy introduced in this work could facilitate the development and application of ingenious mechanochromic materials.

Introduction

Stimuli responsive fluorescent materials display promising prospects by virtue of their wide practical applications, such as chemsensors[1], pH indicators[2], fluorescent probes[3], biosensors[4], photoelectronic devices[5], viscosity probes[6] and mechanochromic materials[7]. In which, mechanochromic materials have attracted intensive attention due to their noteworthy applied value. The phenomenon termed as mechanofluorochromism (MFC) originally referred to as piezochromism or tribochromism reflects color change in response to external force (pressing or grinding), is of significant importance for diverse applications[8]. However, aggregation caused quenching effect (ACQ) is known as an unfavorable phenomenon

that remarkably inhibits the utilization of MFC materials, for the ACQ materials only emit fluorescence in solution instead of solid state[9-11].

Fortunately in 2001, Tang[12] and coworkers first introduced a new concept referred to aggregation induced emission (AIE). These kinds of compounds emit extremely weak fluorescence in solution but intense fluorescence as aggregates form. In 2010, Park[13] first presented cyano distyrylbenzene derivatives that display MFC effect based on AIE property. By virtue of the perfect combination of AIE and MFC materials, number of MFC templates with AIE property are successively reported, including distyrylanthrancene derivatives[14-18], silole derivatives[19], tetraphenylethene (TPE) derivatives[20-25], cyano-substituted diarylethene derivatives[26-28], triphenylamine derivatives[29-31]. However, owing to the lack of clear guidelines for designing molecules possess MFC properties, the study of MFC fluorescent materials is still at the inceptive stage, intensive study and the creation of new templates are just around the corner.

Herein, we report three series of D-π-A 2,6-dimethyl-4-pyrone derivatives (Scheme 1), including 2,6-bis((*E*)-4-alkoxystyryl)-4*H*-pyran-4-one (**PASPs**), 2,6-bis((*E*)-2-alkoxystyryl)-4*H*-pyran-4-one (**OASPs**) and 2,6-bis((*E*)-2-(2-alkoxynaphthalen-l-yl)vinyl)-4*H*-pyran-4-one (**ANPs**). These target compounds based on pyrone skeleton provides new members to AIE family. The MFC feature of these compounds would open a new pathway to fabricate “smart” mechanofluorochromic materials. These compounds show obvious aggregation-induced emission enhancement (AIEE) phenomenon, their fluorescence properties and MFC behavior were investigated using photoluminescence spectra. Furthermore, differential scanning calorimetry (DSC) and powder wide-angle X-ray diffraction (PXRD) were implemented to study the relationship between mechanofluorochromism and structure.

Experimental Section

Materials and characterization

All the raw materials were obtained commercially and used without further

purification. ^{1}H NMR were recorded by using Bruker Avance 400 MHz spectrometer with $CDCl_3$ as solvent. High resolution mass spectrum were measured on Bruker Paltonicsmicro TOF-Q II instrument. IR spectra were recorded using a Nicolet 380 FT-IR spectrometer. Photoluminescence spectra of liquid and photoluminescence spectra of solid were obtained with Hitachi F-2500 spectrophotometer and Horiba Jobin Yvon Fluorolog-3 spectrophotometer, respectively. Powder wide angle X-ray diffraction (PWXD) were recorded on a Miniflex 600 Powder X-ray Diffractometer of Rigaku, with the following instrument parameter: 35V, 15A, 5° min^{-1}. Differential scanning calorimetry (DSC) experiments were operated on a Perkin-Elmerat at a heating rate of 10 ℃ min^{-1}. Annealing experiment: The pressed samples were heated at the temperature of T_m-10 ℃ (T_m is the isotropic melt point of each compound) for 10 min in a muffle furnace.

General procedures for the synthesis of compounds A-n, B-n and C-n

Compounds **A-n**, **B-n** and **C-n** were similarly synthesized according to the literature method[32].

A mixture of hydroxybenzaldehyde (0.010 mol) and K_2CO_3 (1.66 g, 1.20 mol) was added to *N*, *N*-dimethylformamide (20 mL). Alkyl bromide (0.012 mol) was added subsequently. After stirring at 90 ℃ for 8 hours, the mixture was poured into distilled water (200 mL) and extracted with dichloromethane (3×20 mL). The combined organic phases were washed with brine (3×50 mL), dried over Na_2SO_4, concentrated to yield the crude product, which was used for the next step without further purification.

General procedures for PASPs , OASPs and ANPs

Compounds **PASPs**, **OASPs** and **ANPs** were similarly synthesized according to the following procedure.

2,6-dimethyl-4-pyrone (0.31 g, 2.50 mmol) and **B-n** (6.25 mmol) were dissolved in ethyl alcohol (20 mL). Sodium ethoxide (0.43 g, 6.25 mmol) in ethyl alcohol (10 mL) was added dropwise to the above solution. After stirring at 25-40 ℃ for 2 days, 5% hydrochloric acid was employed to adjust the pH of the mixture to 7. The mixture was then extracted with dichloromethane (3×20 mL), the organic phases were washed with

brine (3×50 mL), dried over anhydrous Na_2SO_4, concentrated to afford the crude product. It was purified by column chromatography (petroleum ether/ethyl acetate) and recrystallized in ethyl alcohol to afford the target compound.

2,6-bis((*E*)-4-butoxystyryl)-4*H*-pyran-4-one (**PASP-4**): Yellow solid (0.74 g), 67% yield, m.p. 187-188 ℃. IR (KBr, cm^{-1}): 3040, 2930, 2876, 1643, 1615, 1509, 1391, 1245, 1182, 963, 745. ^{1}H NMR ($CDCl_3$, 400 MHz) δ (ppm) : 7.54 (d, J = 8.4 Hz, 4H), 7.46 (d, J = 16.0 Hz, 2H), 6.97 (d, J = 8.8 Hz, 4H), 6.64 (d, J = 16.0 Hz, 2H), 6.24 (s, 2H), 4.05 (t, J = 12.8 Hz, 4H), 1.85-1.78 (m, 4H), 1.58-1.49 (m, 4H), 1.04 (t, J = 14.8 Hz, 6H). ^{13}C NMR ($CDCl_3$, 100 MHz) δ (ppm): 180.40, 161.39, 160.62, 135.55, 129.09, 127.56, 117.48, 114.96, 113.17, 67.89, 31.24, 19.23, 13.83. HRMS (ESI): calcd for $C_{29}H_{32}O_4$: 467.2193 $(M+Na)^+$, found 467.2195.

2,6-bis((*E*)-4-(octyloxy)styryl)-4*H*-pyran-4-one (**PASP-8**): Brownish yellow solid (1.11 g), 71% yield, m.p. 161-162 ℃. IR (KBr, cm^{-1}): 3031, 2932, 2855, 1644, 1615, 1509, 1391, 1245, 1182, 972, 718. ^{1}H NMR ($CDCl_3$, 400 MHz) δ (ppm) : 7.54 (d, J = 8.8 Hz, 4H), 7.46 (d, J = 16 Hz, 2H), 6.97 (d, J = 8.4 Hz, 4H), 6.64 (d, J = 16 Hz, 2H), 6.24 (s, 2H), 4.04 (t, J = 13.2 Hz, 4H), 1.86-1.79 (m, 4H), 1.51-1.32 (m, 20H), 0.93 (t, J = 13.6 Hz, 6H). ^{13}C NMR ($CDCl_3$, 100 MHz) δ (ppm): 180.39, 161.62, 160.62, 135.54, 129.09, 127.55, 117.48, 114.96, 113.19, 68.21, 31.81, 29.35, 29.23, 29.20, 26.03, 22.65, 14.09. HRMS (ESI): calcd for $C_{37}H_{48}O_4$: 579.3445 $(M+Na)^+$, found 579.3442.

2,6-bis((*E*)-4-(dodecyloxy)styryl)-4*H*-pyran-4-one (**PASP-12**): Brownish yellow solid (1.15 g), 69% yield, m.p. 142-144 ℃. IR (KBr, cm^{-1}): 3040, 2919, 2848, 1647, 1613, 1510, 1401, 1245, 1182, 967, 719. ^{1}H NMR ($CDCl_3$, 400 MHz) δ (ppm): 7.54 (d, J = 8.4 Hz, 4H), 7.46 (d, J = 15.6 Hz, 2H), 6.96 (d, J = 8.4 Hz, 4H), 6.64 (d, J = 16.0 Hz, 2H), 6.24 (s, 2H), 4.04 (t, J = 13.2 Hz, 4H), 1.86-1.79 (m, 4H), 1.49-1.29 (m, 36H), 0.92 (t, J = 13.6 Hz, 6H). ^{13}C NMR ($CDCl_3$, 100 MHz) δ (ppm): 180.40, 161.64, 160.62, 135.55, 129.09, 127.56, 117.49, 114.97, 113.20, 68.22, 31.92, 29.66, 29.63, 29.59, 29.57, 29.38, 29.34, 29.20, 26.02, 22.68, 14.11. HRMS (ESI): calcd for $C_{45}H_{64}O_4$: 691.4697 $(M+Na)^+$, found 691.4691.

2,6-bis((*E*)-2-butoxystyryl)-4*H*-pyran-4-one (**OASP-4**): Yellow solid (0.72 g),

65% yield, m.p. 123-124 ℃. IR (KBr, cm^{-1}): 3067, 2930, 2866, 1640, 1588, 1455, 1391, 1245, 1126, 968, 744. ^{1}H NMR ($CDCl_3$, 400 MHz) δ (ppm): 7.83 (s, 1H), 7.79 (s, 1H), 7.56 (s, 1H), 7.54 (s, 1H), 7.36 (t, *J* = 8.4 Hz, 2H), 7.02-6.96 (m, 6H), 6.22 (s, 2H), 4.11 (t, *J* = 12.8 Hz, 4H), 1.92-1.85 (m, 4H), 1.61-1.51 (m, 4H), 0.98 (t, *J* = 14.8 Hz, 6H). ^{13}C NMR ($CDCl_3$, 100 MHz) δ (ppm): 180.62, 162.00, 157.68, 131.95, 130.77, 128.90, 124.11, 120.76, 120.65, 113.54, 112.13, 68.20, 31.35, 19.43, 13.84. HRMS (ESI): calcd for $C_{29}H_{32}O_4$: 467.2193 $(M+Na)^+$, found 467.2195.

2,6-bis((*E*)-2-(octyloxy)styryl)-4*H*-pyran-4-one (**OASP-8**): Yellow solid (0.90 g), 65% yield, m.p. 86-87 ℃. IR (KBr, cm^{-1}): 3067, 2921, 2848, 1645, 1590, 1463, 1390, 1244, 1126, 990, 970, 742. ^{1}H NMR ($CDCl_3$, 400 MHz) δ (ppm): 7.85 (s, 1H), 7.81 (s, 1H), 7.56 (s, 1H), 7.54 (s, 1H), 7.36 (t, *J* = 16.8 Hz, 2H), 7.02-6.93 (m, 6H), 6.27 (s, 2H), 4.09 (t, *J* = 13.2 Hz, 4H), 1.93-1.86 (m, 4H), 1.54-1.23 (m, 20H), 0.88 (t, *J* = 13.6 Hz, 6H). ^{13}C NMR ($CDCl_3$, 100 MHz) δ (ppm): 180.62, 161.99, 157.67, 131.93, 130.75, 128.77, 124.15, 120.68, 120.66, 113.55, 112.16, 68.57, 31.78, 29.34, 29.29, 29.22, 26.20, 22.59, 14.07. HRMS (ESI): calcd for $C_{37}H_{48}O_4$: 579.3445 $(M+Na)^+$, found 579.3445.

2,6-bis((*E*)-2-(dodecyloxy)styryl)-4*H*-pyran-4-one (**OASP-12**): Yellow solid (1.12 g), 67% yield, m.p. 68-70 ℃. IR (KBr, cm^{-1}): 3040, 2921, 2839, 1641, 1593, 1463, 1381, 1244, 1126, 971, 746. ^{1}H NMR ($CDCl_3$, 400 MHz) δ (ppm): 7.86 (s, 1H), 7.82 (s, 1H), 7.56 (s, 1H), 7.54 (s, 1H), 7.36-7.32 (t, *J* = 16.8 Hz, 2H), 7.02-6.94 (m, 6H), 6.31 (s, 2H), 4.09 (t, *J* = 13.2 Hz, 4H), 1.93-1.86 (m, 4H), 1.54-1.22 (m, 36H), 0.91 (t, *J* = 14 Hz, 6H). ^{13}C NMR ($CDCl_3$, 100 MHz) δ (ppm): 180.59, 161.97, 157.67, 131.91, 130.74, 128.76, 124.15, 120.69, 120.66, 113.56, 112.16, 68.57, 31.92, 29.64, 29.61, 29.60, 29.57, 29.39, 29.34, 29.29, 26.19, 22.69, 14.11. HRMS (ESI): calcd for $C_{45}H_{64}O_4$: 691.4697 $(M+Na)^+$, found 691.4698.

2,6-bis((*E*)-2-(hexadecyloxy)styryl)-4*H*-pyran-4-one (**OASP-16**): Yellow solid (1.21 g), 62% yield, m.p. 52-54 ℃. IR (KBr, cm^{-1}): 3059, 2922, 2840, 1640, 1592, 1464, 1381, 1245, 1127, 970, 744. ^{1}H NMR ($CDCl_3$, 400 MHz) δ (ppm): 7.85 (s, 1H), 7.81 (s, 1H), 7.56 (s, 1H), 7.54 (s, 1H), 7.36 (t, *J* = 15.6 Hz, 2H), 7.02-6.93 (m, 6H), 6.27 (s, 2H), 4.09 (t, *J* = 13.2 Hz, 4H), 1.93-1.86 (m, 4H), 1.33 (m, 52H), 0.92 (t, *J* =

13.6 Hz, 6H). ^{13}C NMR ($CDCl_3$, 100 MHz) δ (ppm): 180.62, 161.98, 157.66, 131.91, 130.74, 128.76, 124.16, 120.70, 120.66, 113.57, 112.15, 68.57, 31.93, 29.69, 29.67, 29.61, 29.57, 29.37, 29.28, 26.19, 22.69, 14.11. HRMS (ESI): calcd for $C_{53}H_{80}O_4$: 803.5949 $(M+Na)^+$, found 803.5956.

2,6-bis((*E*)-2-(naphthalen-l-yl)vinyl)-4*H*-pyran-4-one (**ANP**): Yellow solid (0.75 g), 75% yield, m.p. 192-194 ℃. IR (KBr, cm^{-1}): 3040, 1647, 1557, 1504, 1249, 1168, 953. ^{1}H NMR ($CDCl_3$, 400 MHz) δ (ppm): 8.49 (s, 1H), 8.46 (s, 1H), 8.31 (s, 1H), 8.29 (s, 1H), 7.96 (d, *J* = 7.6 Hz, 4H), 7.90 (d, *J* = 7.2 Hz, 2H), 7.64-7.56 (m, 6H), 6.95 (d, *J* = 16 Hz, 2H), 6.40 (s, 2H). ^{13}C NMR ($CDCl_3$, 100 MHz) δ (ppm): 180.40, 161.19, 133.85, 132.79, 132.16, 131.37, 130.25, 129.03, 126.97, 126.30, 125.66, 124.52, 122.90, 122.22, 114.29. HRMS (ESI): calcd for $C_{29}H_{20}O_2$: 423.1356 $(M+Na)^+$, found 423.1359.

2,6-bis((*E*)-2-(2-butoxynaphthalen-l-yl)vinyl)-4*H*-pyran-4-one (**ANP-4**): Yellow solid (0.99 g), 73% yield, m.p. 186-187 ℃. IR (KBr, cm^{-1}): 3049, 2928, 2866, 1637, 1592, 1562, 1458, 1389, 1264, 1150, 956, 743. ^{1}H NMR ($CDCl_3$, 400 MHz) δ (ppm): 8.33-8.26 (m, 4H), 7.89-7.84 (m, 4H), 7.53 (t, *J* = 8 Hz, 2H), 7.44 (t, *J* = 7.6 Hz, 2H), 7.37 (s, 1H), 7.35 (s, 1H), 7.34 (s, 1H), 7.29 (s, 1H), 6.33 (s, 2H), 4.27 (t, *J* = 12.8 Hz, 4H), 1.94-1.87 (m, 4H), 1.62-1.53 (m, 4H), 0.99 (t, *J* = 14.4 Hz, 6H). ^{13}C NMR ($CDCl_3$, 100 MHz) δ (ppm): 180.85, 162.12, 156.15, 132.89, 131.13, 129.03, 128.80, 128.72, 127.52, 125.10, 123.87, 122.78, 117.08, 113.98, 113.88, 69.13, 31.53, 19.43, 13.79. HRMS (ESI): calcd for $C_{37}H_{36}O_4$: 545.2686 $(M+H)^+$, found 545.2688.

2,6-bis((*E*)-2-(2-(octyloxy)naphthalen-l-yl)vinyl)-4*H*-pyran-4-one (**ANP-8**): Yellow solid (1.15 g), 70% yield, m.p. 102-104 ℃. IR (KBr, cm^{-1}): 3067, 2921, 2848, 1637, 1555, 1510, 1458, 1387, 1264, 1147, 958, 744. ^{1}H NMR ($CDCl_3$, 400 MHz) δ (ppm): 8.33-8.26 (m, 4H), 7.89-7.84 (m, 4H), 7.53 (t, *J* = 7.2 Hz, 2H), 7.44 (t, *J* = 7.6 Hz, 2H), 7.36 (s, 1H), 7.34 (s, 1H), 7.32 (s, 1H), 7.29 (s, 1H), 6.32 (s, 2H), 4.26 (t, *J* = 13.2 Hz, 4H), 1.94-1.87 (m, 4H), 1.55-1.48 (m, 4H), 1.32-1.24 (m, 16H), 0.88 (t, *J* = 13.2 Hz, 6H). ^{13}C NMR ($CDCl_3$, 100 MHz) δ (ppm): 180.78, 162.07, 156.15, 132.88, 131.12, 129.05, 128.81, 128.76, 127.52, 125.09, 123.86, 122.81, 117.12, 114.00, 113.89, 69.50, 31.77, 29.48, 29.28, 29.23, 26.19, 22.61, 14.08. HRMS (ESI): calcd for

$C_{45}H_{52}O_4$: 679.3758 $(M+Na)^+$, found 679.3754.

Results and discussion

Synthesis

Compounds **A-n**, **B-n** and **C-n** were prepared by literature method. The target compounds were easily obtained from the condensation of pyrone with compounds **A-n**, **B-n** and **C-n**, respectively[33]. Their structures were confirmed by ^{1}H NMR, ^{13}C NMR, HRMS and IR. (Fig. S1, S2, S3 and S4 ESI†).

Photophysical properties of PASPs, OASPs and ANPs

In order to determine the AIEE effect of **PASPs**, **OASPs** and **ANPs**, their fluorescence in solution was studied using THF and water as good and poor solvent, respectively. In molecularly dissolved solution, molecules exist in a relative random way which can result in weaker intermolecular hydrogen bonding and steric hinderance. In this regard, the intramolecular torsion is relatively free, which accelerate the nonradiative pathway and affords weak fluorescence[34,35]. Adding water to the well-dissolved system can result in the formation of aggregates and further lead to changes of their photoluminescence (PL) spectra. As shown in Fig.1 (Fig. S5, ESI†), the THF solution of **OASP-4** (1×10^{-5} mol L^{-1}) emitted weak blue fluorescence originally. As expected, this nonradiative relaxation pathway is possibly ascribed to the free rotation of the phenyl ring around single bond. Along with the increase of water fraction (f_w), the fluorescence intensity of **OASP-4** increased gradually and was accompanied with large bathochromic shift. The corresponding emission peak showed nearly 126 nm red shift until reaching the maximum PL intensity at 70% water fraction. This phenomenon may be related to the transformation from the locally excited state (LE) to the twisted intramolecular charge transfer state (TICT) along with the increase of solvent polarity which can be confirmed by solvatochromic experiment (Fig. 2). It usually occurs in the molecules containing electron donor and acceptor. Solvation effect stabilizing HOMO and LOMO orbits simultaneously but more to LOMO, thus give rise to a narrowed band

gap and a red-shifted emission spectrum[36,37]. Moreover, the PL intensity of **OASP-4** was 18 times larger than that in pure THF due to the restriction of intramolecular rotation (RIR). When water was added, the molecules began to aggregate in the limited space and the free rotation was blocked to some extent, further facilitating the radiative relaxation pathway and afford enhanced emission[38-40]. Moreover, hydrogen bonds were considered to enhance the molecular rigidity which may also contribute to fluorescence enhancement. However, further addition of water results in the reduction of fluorescence intensity. When f_w exceeds 70%, parts of the molecules begun to assemble into amorphous aggregates to yield a mixture of crystalline and amorphous particles and result in weak luminescent[41-43]. Surprisingly, further incorporation of water led to blue-shifted PL spectra, but the reason remained unclear. All of the **PASPs**, **OASPs** and **ANPs** derivatives showed similar luminescent phenomenon apart from a few exceptions. The PL intensity might depend on the aggregate stages and shows a complex phenomenon at different stages.

On account of their D-π-A structures, solvatochromic property was examined. As described in Fig.2, the florescence spectra showed a gradual red shift as the solvent changed from cyclohexane to DMF, exhibited 44 nm, 36 nm, 42 nm spectra shift for **OASP-8**, **PASP-8** and **ANP-8**, respectively. These changes are ascribed to larger dipole moment and charge separation degree in the exited state than that in the ground state[44]. Obvious intramolecular charge transfer (ICT) characteristics were verified in these compounds.

Mechanochromic properties

The mechanochromic properties of **OASPs**, **PASPs** and **ANPs** were examined upon grinding using a mortar and pestle. The typical PL spectra upon external pressure are illustrated in Fig.3 (Fig. S6, ESI†) with fluorescence images embedded inside. It was found that **OASP-8**, **PASP-12** and **ANP-8** exhibited blue, dark green and yellow fluorescence, respectively. Upon mechanical stimuli, all of them displayed obvious color changes and turned into cyan, brownish yellow and orange yellow. The

resultant red shift is attributed to the planarization induced by grinding. In general, AIE molecules usually adopt a twisted configuration owing to the steric hindrance between moieties. The loose packing mode can lead to the formation of intermolecular cavities. When the samples are pressed, the binding energy released, accompanied by the destruction of crystal lattice. In this regard, configuration planarization gave rise to a red-shifted fluorescence spectra[45].

To deeply understand the fluorescence property, all the corresponding spectroscopic data were summarized in Table 1. As we can see, the mechanochromic property showed a zigzag tendency along with the chain length and reached its maximum at **OASP-8** ($\Delta\lambda_{PFC} = \lambda_{ground}-\lambda_{annealed}$ = 20 nm). The shrink of $\Delta\lambda_{PFC}$ can be attributed to the bulky alkyl group located in the ortho position. The intramolecular steric hindrance impeded the typical planarization to afford inferior mechanochromic property. However, for **PASPs**, the longer the chain length, the more conspicuous the MFC to be induced by grinding. Molecules with longer alkyl chain may adopted a more twisted backbone to provide cavity and loose stacking mode. Therefore, mechanical force can induce a more obvious red shift. For **ANPs** molecules, the presented MFC property stems from the combination of the above two forces.

PXRD and DSC experiment

To further confirm the packing mode of the original and ground form of the present compounds, powder X-ray diffraction (PXRD) and differential scanning calorimetry (DSC) were performed. As shown in Fig. 4 (Fig. S7, ESI†), the diffraction pattern of the original **OASP-4**, **PASP-4** and **ANP-4** exhibit multiple sharp and intense reflections which manifest regular micro-crystalline conformation. In contrast, the XRD profile of the ground state displayed weak and broad diffractograms. This is because of the destruction of a somewhat crystalline phase and the formation of a disordered amorphous state[46]. These results provided convincing evidence among the molecular packing mode and the MFC property.

The thermal properties of **OASP-4**, **PASP-4** and **ANP-4** were investigated by

differential scanning calorimetry (DSC). As described in Fig.5 (Fig. S8, ESI†), **OASP-4** has one endothermic peak, while both of the **PASP-4** and **ANP-4** display three endothermic peaks. In general, the maximum endothermic peak can be realized as the isotropic melt transition (T_m) and there is no change upon grinding. Furthermore, it is easy to find that the T_m decreases with the increase of chain length. This phenomenon could be ascribed to the loose packing mode and weak intermolecular interaction. However, it is unexpected that all of these compounds display no exothermic cold crystallization peak in the ground state. The endothermic peak in the low-temperature zone are considered to be the transformation from solid state to liquid crystalline (T_L) state. It is noted that T_L of **ANP-4** and **PASP-4** shifted from 106℃ to 113℃ and from 102℃ to 136℃ respectively after grinding with the peaks became broad and flat accordingly. Moreover, the two melting endotherm peaks lied in **PASP-4** can be attributed to the recrystallization procedure in a slow heating process. In which, the incomplete crystals with low melting temperature can recrystallize into more perfect lamellae to present a “double melting” phenomenon[47] . To sum up, there is little relationship between MFC property and phase transformation.

Conclusion

In this work, three series of D-π-A compounds **OASPs**, **PASPs** and **ANPs** with AIEE property were designed and successfully synthesized. These compounds exhibited solvatochromism: the fluorescence spectra red-shifted with the increase of solvent polarity. Interestingly, all of these compounds exhibit red-shifted MFC properties, in which, **PASP-12** displayed the largest MFC spectra shift ($\Delta\lambda_{PFC}$ = 23nm). It was found that the MFC properties were distinctly position and alkyl-length dependent. For **PASPs** and **ANPs**, the longer the alkyl chain, the more remarkable MFC properties displayed. While for **OASPs**, the MFC characteristic showed an inverted U-shaped tendency. All the ground state can be recovered completely or partly through an annealing process. PXRD and DSC revealed that the MFC mechanism was ascribed to the transformation among crystalline state and the

amorphous state by grinding. We believe the work presented here can provide new strategy for designing new MFC templates based on AIE.

Acknowledgement

We are grateful for the financial support from the National Natural Science Foundation of China (21576194).

Reference

[1] Zhang Y, Xia J, Feng X, Tong B, Shi J, Zhi, J, et al. Applications of self-assembled one-bilayer nanofilms based on hydroxyl-containing tetraphenylethene derivative's nanoaggregates as chemosensors to volatile of solid nitroaromatics. Sensors Actuat B-Chem 2012;161:587-93.

[2] Chen S, Liu J, Liu Y, Su H, Hong Y, Jim CKW, et al. An AIE-active hemicyanine fluorogen with stimuli-responsive red/blue emission: extending the pH sensing range by “switch + knob” effect. Chem SCI 2012;3:1804-9.

[3] Mandal K, Jana D, Ghorai BK, Jana NR. Fluorescent Imaging Probe from Nanoparticle Made of AIE Molecule. J Phys Chem C 2016;120:5196−206.

[4] Han K, Wang S, Lei Q, Zhu J, Zhang X. Ratiometric Biosensor for Aggregation-Induced Emission-Guided Precise Photodynamic Therapy. ACS Nano 2015; 9:10268-77.

[5] Liu B, Nie H, Zhou X, Hu S, Luo D, Gao D, et al. Manipulation of Charge and Exciton Distribution Based on Blue Aggregation-Induced Emission Fluorophors: A Novel Concept to Achieve High-Performance Hybrid White Organic Light-Emitting Diodes. Adv Funct Mater 2016;26:776-83.

[6] Telore RD, Satam MA, Sekar N. Push-pull fluorophores with viscosity dependent and aggregation induced emissions insensitive to polarity. Dyes Pigm 2015;122: 359-67.

[7] Meng X, Qi G, Zhang C, Wang K, Zou B, Ma Y. Visible mechanochromic responses of spiropyrans in crystals via pressure-induced isomerization. Chem Commun 2015;51:9320-3.

[8] Peebles C, Wight CD, Iverson BL. Solution- and solid-state photophysical and stimuli-responsive behavior in conjugated monoalkoxynaphthalene–naphthalimide donor–acceptor dyads. J Mater Chem C 2015;3:12156-63.

[9] Shi J, Chang N, Li C, Mei J, Deng C, Luo X, et al. Locking the phenyl rings of tetraphenylethene step by step: understanding the mechanism of aggregation-induced emission. Chem Commun 2012;48:10675-7.

[10] Xue P, Sun J, Chen P, Gong P, Yao B, Zhang Z, et al. Strong solid emission and mechanofluorochromism of carbazole-based terephthalate derivatives adjusted by alkyl chains. J Mater Chem C 2015;3:4086-92.

[11] Zheng H, Li C, He C, Dong Y, Liu Q, Qin P, et al. Luminescent hydrogels based on di(4-propoxyphenyl)-dibenzofulvene exhibiting four emission colours and organic solvents/thermal dual-responsive properties. J Mater Chem C 2014;2:5829-35.

[12] Tang B, Zhan X, Yu G, Lee PPS, Liu Y, Zhu D. Efficient blue emission from siloles. J Mater Chem 2001;11:2974-8.

[13] Yoon SJ, Chung JW, Gierschner J, Kim KS, Choi MG, Kim D, et al. Multistimuli Two-Color Luminescence Switching via Different Slip-Stacking of Highly Fluorescent Molecular Sheets. J Am Chem Soc 2010;132:13675-83.

[14] Xiong Y, Yan X, Ma Y, Li Y, Yin G, Chen L. Regulating the piezofluorochromism of 9,10-bis(butoxystyryl)anthracenes by isomerization of butyl groups. Chem Commun 2015;51:3403-6.

[15] Zheng M, Zhang D, Sun M, Li Y, Liu T, Xue S, et al. Cruciform 9,10-distyryl-2,6-bis(p-dialkylaminostyryl) anthracene homologues exhibiting alkyl length-tunable piezochromic luminescence and heat-recovery temperature of ground states. J Mater Chem C 2014;2:1913-20.

[16] Liu W, Wang J, Gao Y, Sun Q, Xue S, Yang W. 2,6,9,10-Tetra(*p*-dibutylaminostyryl)anthracene as a multifunctional fluorescent cruciform dye. J Mater Chem C 2014;2:9028-34.

[17] Xue S, Liu W, Qiu X, Gao Y, Yang W. Remarkable Isomeric Effects on Optical and Optoelectronic Properties of N‑Phenylcarbazole-Capped 9,10-Divinylanthracenes. J Phys Chem C 2014;118:18668-75.

[18] Niu C, You Y, Zhao L, He D, Na N, Ouyang J. Solvatochromism, Reversible Chromism and Self-Assembly Effects of Heteroatom-Assisted Aggregation-Induced Enhanced Emission (AIEE) Compounds. Chem Eur J 2015;21:13983-90.

[19] Chang Z, Jing L, Wei C, Dong Y, Ye Y, Zhao Y, et al. Hexaphenylbenzene-Based, π-Conjugated Snowflake-Shaped Luminophores: Tunable Aggregation-Induced Emission Effect and Piezofluorochromism. Chem Eur J 2015; 21:8504 -10.

[20] Tong J, Wang Y, Mei J, Wang J, Qin A, Sun J, et al. A 1,3-Indandione-Functionalized Tetraphenylethene: Aggregation-Induced Emission, Solvatochromism, Mechanochromism, and Potential Application as a Multiresponsive Fluorescent Probe. Chem Eur J 2014;20:4661-70.

[21] Qi Q, Qian J, Tan X, Zhang J, Wang L, Xu B, et al. Remarkable Turn-On and Color-Tuned Piezochromic Luminescence: Mechanically Switching Intramolecular Charge Transfer in Molecular Crystals. Adv Funct Mater 2015;25:4005–10.

[22] Zhao L, Lin Y, Liu T, Li H, Xiong Y, Yuan W, et al. Rational bridging affording luminogen with AIE features and high field effect mobility. J Mater Chem C 2015;3: 4903-9.

[23] Yu CYY, Kwok RTK, Mei J, Hong Y, Chen S, Lam JWY et al. A tetraphenylethene-based caged compound: synthesis, properties and applications. Chem Commun 2014;50:8134-6.

[24] Yang Z, Qin W, Leung NLC, Arseneault M, Lam JWY, Liang G, et al. A mechanistic study of AIE processes of TPE luminogens: intramolecular rotation vs. configurational isomerization. J Mater Chem C 2016;4:99-107.

[25] Hu T, Yao B, Chen X, Li W, Song Z, Qin A, et al. Effect of ionic interaction on the mechanochromic properties of pyridinium modified tetraphenylethene. Chem Commun 2015;51:8849-52.

[26] Shen X, Wang Y, Zhao E, Yuan W, Liu Y, Lu P, et al. Effects of Substitution with Donor−Acceptor Groups on the Properties of Tetraphenylethene Trimer: Aggregation-Induced Emission, Solvatochromism, and Mechanochromism. J Phys Chem C 2013;117:7334-47.

[27] Zhang X, Ma Z, Yang Y, Zhang X, Jia X, Wei Y. Fine-tuning the mechanofluorochromic properties of benzothiadiazole-cored cyano-substituted diphenylethene derivatives through D–A effect. J Mater Chem C 2014;2:8932-8.

[28] Lu Q, Li X, Li J, Yang Z, Xu B, Chi Z, et al. Influence of cyano groups on the properties of piezofluorochromic aggregation-induced emission enhancement compounds derived from tetraphenylvinyl-capped ethane. J Mater Chem C 2015;3: 1225-34.

[29] Cao Y, Xi W, Wang L, Wang H, Kong L, Zhou H, et al. Reversible piezofluorochromic nature and mechanism of aggregation-induced emission-active compounds based on simple modification. RSC Adv 2014;4:24649-52.

[30] Zhang Y, Sun J, Zhuang G, Ouyang M, Yu Z, Cao F, et al. Heating and mechanical force-induced luminescence on–off switching of arylamine derivatives with highly distorted structures. J Mater Chem C 2014;2:195-200.

[31] Zhang Y, Sun J, Lv X, Ouyang M, Cao F, Pan G, et al. Heating and mechanical force-induced “turn on” fluorescence of cyanostilbene derivative with H-type stacking. CrystEngComm 2013;15:8998-9002.

[32] Xiong Y, Ma Y, Yan X, Yin G, Chen L. Significant effect of alkyl chain length on fluorescent thermochromism of 9,10-bis(*p*-alkoxystyryl)anthracenes. RSC Adv 2015; 5:53255-8.

[33] Ghandi M, Bayat Y, Teimuri-Mofrad R. A novel method for the synthesis of formyl and hydroxymethyl derivatives of 4*H*-pyran-4-one. Org Prep Proced Int 2002; 34:525-30.

[34] Sun Q, Liu W, Ying S, Wang L, Xue S, Yang W. 9,10-Bis(N-alkylindole-3-yl-vinyl-2)anthracenes as a new series of alkyl length-dependent piezofluorochromic aggregation-induced emission homologues. RSC Adv 2015;5:73046-50.

[35] Li L, Chen M, Zhang H, Nie H, Sun J, Qin A, et al. Influence of the number and substitution position of phenyl groups on the aggregation-enhanced emission of benzene-cored luminogens. Chem Commun 2015;51:4830-3.

[36] Hu R, Lager E, Aguilar-Aguilar A, Liu J, Lam JWY, Sung HHY, et al. Twisted

Intramolecular Charge Transfer and Aggregation-Induced Emission of BODIPY Derivatives. J Phys Chem C 2009;113:15845-53.

[37] Zhang Y, Sun J, Bian G, Chen Y, Ouyang M, Hu B, et al. Cyanostilben-based derivatives: mechanical stimuli-responsive luminophors with aggregation-induced emission enhancement. Photochem Photobiol Sci 2012;11:1414-21.

[38] Huang W, Tang F, Li B, Su J, Tian H. Large cyano- and triazine-substituted D–π–A–π–D structures as efficient AIEE solid emitters with large two-photon absorption cross sections. J Mater Chem C 2014;2:1141-8.

[39] Bu L, Sun M, Zhang D, Liu W, Wang Y, Zheng M, et al. Solid-state fluorescence properties and reversible piezochromic luminescence of aggregation-induced emission-active 9,10-bis[(9,9-dialkylfluorene-2-yl)vinyl] anthracenes. J Mater Chem C 2013;1:2028-35.

[40] Chen L, Jiang Y, Nie H, Hu R, Kwok HS, Huang F, et al. Rational Design of Aggregation-Induced Emission Luminogen with Weak Electron Donor−Acceptor Interaction to Achieve Highly Efficient Undoped Bilayer OLEDs. Appl Mater Interfaces 2014;6:17215-25.

[41] Liu Y, Lei Y, Li F, Chen J, Liu M, Huang X, et al. Indene-1,3-dionemethylene-4*H*-pyran derivatives containing alkoxy chains of various lengths: aggregation-induced emission enhancement, mechanofluorochromic properties and solvent-induced emission changes. J Mater Chem C 2016;4:2862-70.

[42] Luo X, Li J, Li C, Heng L, Dong Y, Liu Z, et al. Reversible Switching of the Emission of Diphenyldibenzofulvenes by Thermal and Mechanical Stimuli. Adv Mater 2011;23:3261-5.

[43] Chen M, Li L, Nie H, Tong J, Yan L, Xu B, et al. Tetraphenylpyrazine-based AIEgens: facile preparation and tunable light emission. Chem Sci 2015;6:1932–7.

[44] Xue P, Yao B, Sun J, Xu Q, Chen P, Zhang Z, et al. Phenothiazine-based benzoxazole derivates exhibiting mechanochromic luminescence: the effect of a bromine atom. J Mater Chem C 2014;2:3942–50.

[45] Zhang X, Chi Z, Zhang J, Li H, Xu B, Li X, et al. Piezofluorochromic Properties and Mechanism of an Aggregation-Induced Emission Enhancement Compound

Containing *N*-Hexyl-phenothiazine and Anthracene Moieties. J Phys Chem B 2011; 115:7606–11.

[46] Cui Y, Yin Y, Cao H, Zhang M, Shan G, Sun H, et al. Efficient piezochromic luminescence from tetraphenylethene functionalized pyridine-azole derivatives exhibiting aggregation-induced emission. Dyes Pigm 2015;119:62-9.

[47] Jin L, Ball J, Bremner T, Sue H. Crystallization behavior and morphological characterization of poly(ether ether ketone). Polymer 2014;55:5255-65.

Caption of figures

Scheme 1. Synthesis and structures of **OASPs**, **PASPs** and **ANPs**

Figure 1. PL spectra of the compounds in water/THF mixtures

(A) **PASP-4**; (B) **OASP-4**; (C) **ANP** (concentration, 10^{-5} mol L^{-1}; excitation wavelength,

PASP-4: 320 nm; **OASP-4**: 330 nm; **ANP**: 340 nm)

The insets depict the changes in PL peak intensity and emission images of the compound in different water fraction mixtures under 365 nm UV illumination

Figure 2. PL spectra of **ANP-8**, **PASP-8** and **OASP-8** in different solvents with varying polarities (concentration, 10^{-4} mol L^{-1}; excitation wavelength,

ANP-8: 365 nm; **OASP-8**: 330 nm; **PASP-8**: 320 nm)

The insets depict the emission images of the compounds in cyclohexane, toluene, THF, CH_2Cl_2, DMF (from left to right) under 365 nm UV illumination

Figure 3. Normalized fluorescence emission spectra of **ANP-8**, **PASP-12**, **OASP-8** samples mixed with KBr upon grinding, annealing.

The insets depict the fluorescence images of **ANP-8**, **PASP-12**, **OASP-8**, samples taken at 365 nm UV lamp after grinding and annealing.

Figure 4. Powder wide-angle X-ray diffraction (PXRD) patterns of **PASP-4**, **ANP-4** and **OASP-4** in original and ground states

Figure 5. Differential Scanning Calorimetry (DSC) curves of **PASP-4**, **ANP-4** and **OASP-4** in original and ground states

Caption of table

Table 1 Peak emission wavelength (nm) of solid-state **OASPs**, **PASPs** and **ANPs** derivatives under different conditions

Table 1 Peak emission wavelength (nm) of solid-state **OASPs**, **PASPs** and **ANPs** derivatives under different conditions

Samples	$\lambda_{original}$	$\lambda_{pressed}$	$\lambda_{annealed}$	$\Delta\lambda_{PFC}$
OASP-4	466	478	464	14
OASP-8	458	478	458	20
OASP-12	455	472	460	12
OASP-16	442	473	465	8
PASP-4	490	508	493	15
PASP-8	460	500	481	19
PASP-12	472	503	480	23
ANP	505	514	504	10
ANP-4	517	524	513	11
ANP-8	516	526	512	14

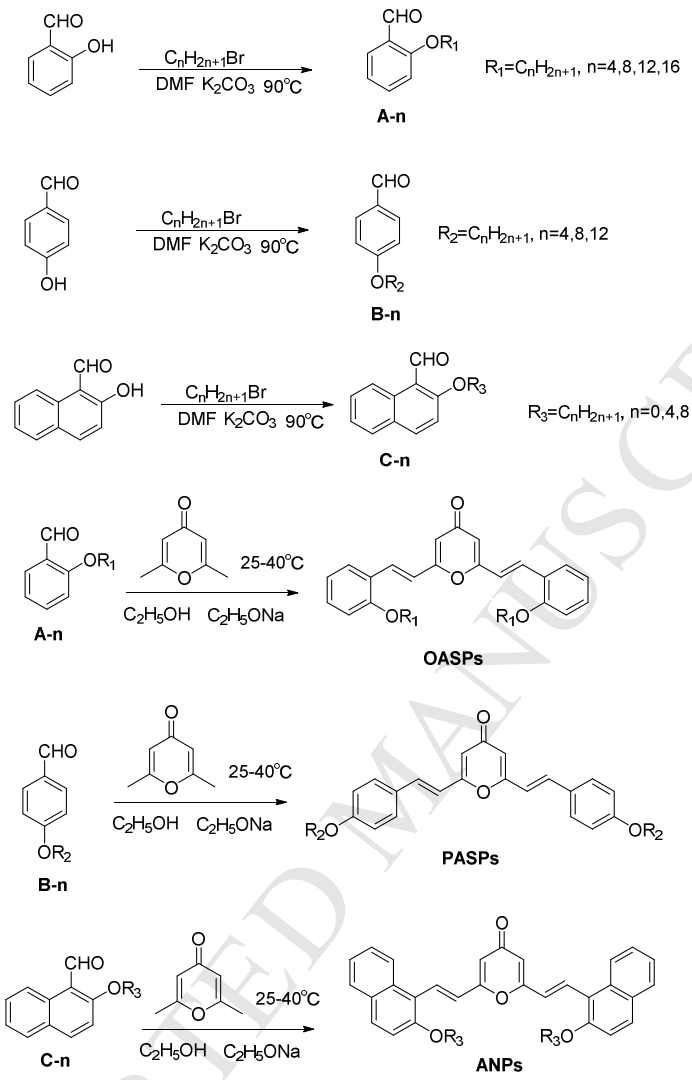

Scheme 1. Synthesis and structures of **OASPs**, **PASPs** and **ANPs**

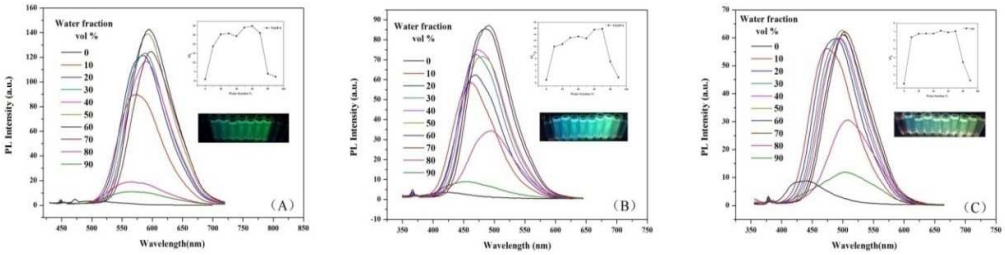

Figure 1. PL spectra of the compounds in water/THF mixtures

(A) **PASP-4**; (B) **OASP-4**; (C) **ANP** (concentration, 10^{-5} mol L^{-1}; excitation wavelength, **PASP-4**: 320 nm; **OASP-4**: 330 nm; **ANP**: 340 nm)

The insets depict the changes in PL peak intensity and emission images of the compound in different water fraction mixtures under 365 nm UV illumination

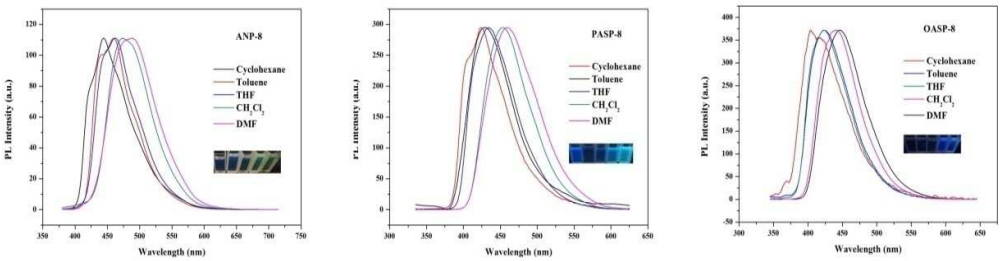

Figure 2. PL spectra of **ANP-8**, **PASP-8** and **OASP-8** in different solvents with varying polarities (concentration, 10^{-4} mol L^{-1}; excitation wavelength,

ANP-8: 365 nm; **OASP-8**: 330 nm; **PASP-8**: 320 nm)

The insets depict the emission images of the compounds in cyclohexane, toluene, THF, CH_2Cl_2, DMF (from left to right) under 365 nm UV illumination

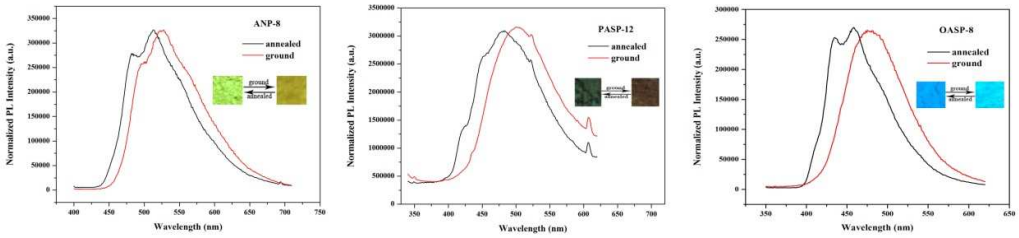

Figure 3. Normalized fluorescence emission spectra of **ANP-8**, **PASP-12**, **OASP-8** samples mixed with KBr upon grinding, annealing.

The insets depict the fluorescence images of **ANP-8**, **PASP-12**, **OASP-8**, samples taken at 365nm UV lamp after grinding and annealing.

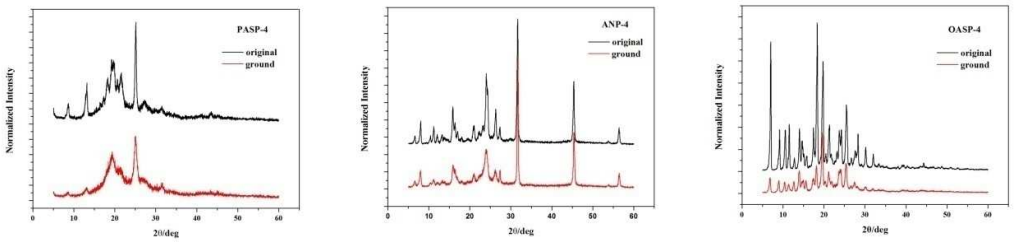

Figure 4. Powder wide-angle X-ray diffraction (PXRD) patterns of **PASP-4**, **ANP-4** and **OASP-4** in original and ground states

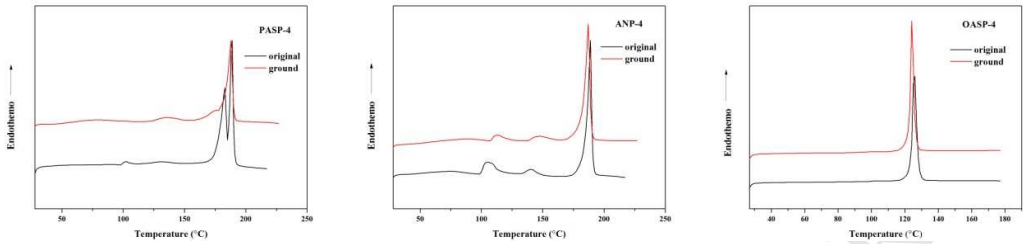

Figure 5. Differential Scanning Calorimetry (DSC) curves of **PASP-4**, **ANP-4** and **OASP-4** in original and ground states

Highlights

The synthesized new AIE templates exhibit obvious mechanochromic behavior.
D-π-A 2, 6-dimethyl-4-pyrone-cored derivatives present AIEE and solvatochromism.
Mechanochromic behavior was mainly depended on substituents' position and length.